# Silver pyrazole complexes with tunable liquid crystals and luminescent properties†

**María José Mayoral,[a] Paloma Ovejero,[a] José Antonio Campo,[a] José Vicente Heras,[a] María Rosario Torres,[b] Carlos Lodeiro*[c] and Mercedes Cano*[a]**

***Received (in Gainesville, FL, USA) 11th December 2009, Accepted 11th June 2010***
**DOI: 10.1039/b9nj00753a**



New silver ionic complexes based on pyrazole ligands of the type $[Ag(Hpz^{2R(n)})_2][A]$ ($Hpz^{2R(n)}$ = 3,5-bis(4-alkyloxyphenyl)pyrazole; R = $C_6H_4OC_nH_{2n+1}$; [A] = $CH_3$-*p*-$C_6H_4SO_3^-$ (PTS), $CF_3SO_3^-$ (OTf)) (type **I**) are liquid crystal materials exhibiting photoluminescence in the solid state, in solution and in the mesophase. By way of contrast, the related counterparts $[Ag(Hpz^{R(n)})_2][A]$ ($Hpz^{R(n)}$ = 3-(4-alkyloxyphenyl)pyrazole; R = $C_6H_4OC_nH_{2n+1}$; [A] = $CH_3$-*p*-$C_6H_4SO_3^-$ (PTS), $CF_3SO_3^-$ (OTf)) (type **II**), containing monosubstituted pyrazole ligands, are not mesomorphic but also behave as luminescent materials. The crystalline structures of **5** and **10**, as representative examples of classes **I** and **II**, have been solved. Molecular "H" or "Z" shapes, depending on the *cis* or *trans* orientation of the NH groups of the pyrazole ligands, were found, respectively. The first type gave rise to a layer-planar network, while a corrugated layer was found for complex **10**, these features being related to the mesomorphic behaviour of both kinds of compounds. The mesomorphic and luminescent properties of complexes **I** and **II** were compared with those of related compounds containing the less sterically-demanding counteranions $PF_6^-$, $NO_3^-$ and $BF_4^-$, described in our previous work. In all cases, the effect of the counteranions, as well as the substitution on the pyrazole groups, were analyzed for their corresponding properties.

## Introduction

The design of molecular materials, in which light emission or charge-transport properties are combined with a supramolecular organisation, could be a good strategy in order to attain the required improvements demanded by electro-optic devices for practical applications (displays, solar cells, data treatment and storage date, image components).[1] In this context, luminescent liquid crystals could be used as multifunctional materials on the basis that they combine luminescence with the ordering of fluid phases.[2,3]

The interest in liquid crystal materials as a support for the modern technology of LCDs demands an increase of their research, which is especially evident in cost-saving color LCD displays. These devices present several limitations, such as low brightness and energy efficiency, due to the use of polarisers and color filters, which transform a great part of the incident light into thermal energy.[4] One way to overcome this shortcoming could be the use of luminescent liquid crystals.

On designing luminescent mesophases, metallomesogens offer an interesting opportunity. They combine liquid crystal properties with the characteristics of the metal ions they contain; therefore, the typical photoluminescent behaviour of selected metal complexes can be used as a support for extending those properties to related metallomesogens.[5]

In particular, looking for new luminescent liquid crystal materials, appropriately designed gold(I) and silver(I) complexes can be considered good choices. Gold and silver complexes frequently possess luminescence, this behaviour being usually, but not necessarily, associated with the presence of metal–metal interactions.[6] Then, it is possible to suggest that in the liquid crystal state, the supramolecular ordering of mesophases could contribute to overtake metal–metal interactions, and in this way favour the luminescence properties.

Since the report of the first luminescent metallomesogens of gold(I),[7] there have been growing developments in this type of molecular material based specially on lanthanide ions,[4,5,8–12] and to a lesser extent transition metals such as Pd,[13] Ni,[14] Pt,[15,16] Zn,[17,18] Cu,[19] Ag[20] and Au.[21]

Very recently, we have reported a series of ionic silver(I) and gold(I) mesomorphic complexes based on pyrazole type ligands containing long-chained alkyloxyphenyl R-substituents (R = $C_6H_4OC_nH_{2n+1}$), and $PF_6^-$, $NO_3^-$ and $BF_4^-$ counteranions, which exhibit an intense photoluminescent behaviour in the solid state, in solution, as well as in the mesophase.[22]

[a] *Departamento de Química Inorgánica I, Facultad de Ciencias Químicas, Universidad Complutense, E-28040 Madrid, Spain. E-mail: mmcano@quim.ucm.es*
[b] *Laboratorio de Difracción de Rayos-X, Facultad de Ciencias Químicas, Universidad Complutense, E-28040 Madrid, Spain*
[c] *Grupo BIOSCOPE, Departamento de Química-Física, Facultade de Ciencias, Campus de Ourense, Universidade de Vigo, 32004 Ourense, Spain. E-mail: clodeiro@uvigo.es*

† Electronic supplementary information (ESI) available: Selected lengths, angles and hydrogen-bond geometries for **5** and **10** (Tables S1–S4), together with analytical data of the compounds (Table S5). In addition, Fig. S1 shows the ORTEP plot of the asymmetric unit of **10**. CCDC deposition numbers 756790 (**5**) and 756791 (**10**). For crystallographic data in CIF or other electronic format see DOI: 10.1039/b9nj00753a

 

We have proved that, independent of the nature of mesomorphic $Hpz^{2R(n)}$ ($Hpz^{2R(n)}$ = 3,5-bis(4-alkyloxyphenyl)pyrazole) or non-mesomorphic $Hpz^{R(n)}$ ($Hpz^{R(n)}$ = 3-(4-alkyloxyphenyl)-pyrazole) ligands, they are able to induce mesomorphism upon coordination to Ag(I) and Au(I) fragments. The non-conventional "H" molecular shape and supramolecular ordering found in these complexes in the solid state are related to liquid crystalline behaviour.

In order to modify and hopefully improve the liquid crystal and luminescence properties of this kind of compound, in this work, we have extended our studies to ionic pyrazole-Ag(I) complexes by using coordinative and sterically-demanding counteranions such as $CH_3$-*p*-$C_6H_4SO_3^-$ (PTS) and $CF_3SO_3^-$ (OTf). In these systems, the influence of the counteranions on the structural characteristics, as well as the photoluminescence and liquid crystal properties, is studied and compared with those of the related counterparts above-mentioned.[22]

## Results and discussion

### Synthesis and characterisation

The Ag(I) complexes of the type **I** $[Ag(Hpz^{2R(n)})_2][A]$ ([A] = $CH_3$-*p*-$C_6H_4SO_3^-$ (PTS) (**1–4**), $CF_3SO_3^-$ (OTf) (**5–9**)) and type **II** $[Ag(Hpz^{R(n)})_2][A]$ ([A] = $CH_3$-*p*-$C_6H_4SO_3^-$ (PTS) (**10–14**) and $CF_3SO_3^-$ (OTf) (**15–18**)) were prepared by reaction of the pyrazole ligands $Hpz^{2R(n)}$ or $Hpz^{R(n)}$ with the corresponding silver salt AgA in a 2 : 1 molar ratio (Scheme 1, Table 1). All compounds were isolated as white solids, and characterised by elemental analysis (C, H, N) and spectroscopic techniques (IR and $^1$H NMR) (see the Experimental section). Matrix-assisted laser desorption/ionization time-of-flight mass spectrometry (MALDI-TOF-MS) was also used for complexes **1**, **7** and **11**.

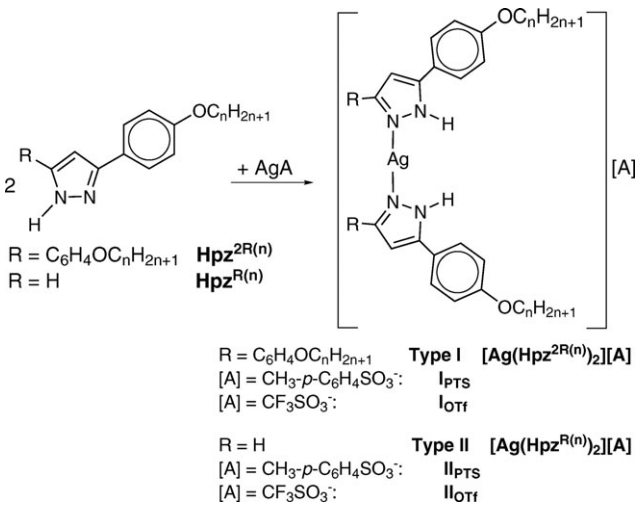


**Scheme 1** Schematic synthesis.

The $^1$H NMR spectra of all the compounds in a $CDCl_3$ solution at room temperature exhibited characteristic signals of the alkyloxyphenyl ($C_6H_4OC_nH_{2n+1}$)-substituted pyrazole ligands (Fig. 1). The presence of only one set of signals of each type of proton is in agreement with the equivalence of the two pyrazoles, as well as their substituents, this feature being explained in terms of a metallotropic equilibrium similar to that previously found for related complexes.[23,24] On the other hand, the absence of the NH-pyrazolic signal suggests the presence of strong H-bond interactions. The resonances of the alkyl protons of the $C_6H_4OC_nH_{2n+1}$ substituents appear in the expected regions, not being influenced by the chain length.

The IR spectra in the solid state show, among other bands, the characteristic bands of the pyrazole ligands and those of the corresponding counteranions. As a general pattern, an absorption band is observed at *ca.* 1600 $cm^{-1}$, associated with $\nu$(C=N) and $\nu$(C=C) vibrations, and a sharp $\nu$(NH) band at *ca.* 3100–3300 $cm^{-1}$.[25] The values of the $\nu$(NH) bands agree with those observed in several complexes containing

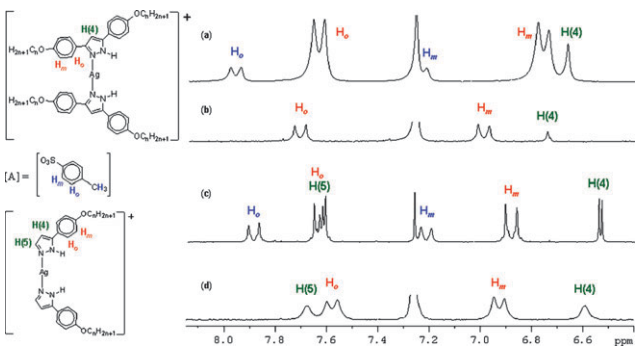


**Fig. 1** The aromatic region of the $^1$H NMR spectra of complexes (a) $[Ag(Hpz^{2R(12)})_2][CH_3$-*p*-$C_6H_4SO_3]$ (**1**), (b) $[Ag(Hpz^{2R(12)})_2][CF_3SO_3]$ (**6**), (c) $[Ag(Hpz^{R(12)})_2][CH_3$-*p*-$C_6H_4SO_3]$ (**11**) and (d) $[Ag(Hpz^{R(12)})_2]$-$[CF_3SO_3]$ (**15**) in $CDCl_3$.

**Table 1** Classification of the complexes, including their numbering

| $[Ag(Hpz^{2R(n)})_2][A]$ | | | | $[Ag(Hpz^{R(n)})_2][A]$ | | | |
|---|---|---|---|---|---|---|---|
| Number | *n* | A | Type I | Number | *n* | A | Type II |
| | | | | **10** | 1 | $CH_3$-*p*-$C_6H_4SO_3^-$ | |
| **1** | 12 | $CH_3$-*p*-$C_6H_4SO_3^-$ | $\mathbf{I_{PTS}}$ | **11** | 12 | $CH_3$-*p*-$C_6H_4SO_3^-$ | $\mathbf{II_{PTS}}$ |
| **2** | 14 | $CH_3$-*p*-$C_6H_4SO_3^-$ | | **12** | 14 | $CH_3$-*p*-$C_6H_4SO_3^-$ | |
| **3** | 16 | $CH_3$-*p*-$C_6H_4SO_3^-$ | | **13** | 16 | $CH_3$-*p*-$C_6H_4SO_3^-$ | |
| **4** | 18 | $CH_3$-*p*-$C_6H_4SO_3^-$ | | **14** | 18 | $CH_3$-*p*-$C_6H_4SO_3^-$ | |
| **5** | 1 | $CF_3SO_3^-$ | $\mathbf{I_{OTf}}$ | | | | $\mathbf{II_{OTf}}$ |
| **6** | 12 | $CF_3SO_3^-$ | | **15** | 12 | $CF_3SO_3^-$ | |
| **7** | 14 | $CF_3SO_3^-$ | | **16** | 14 | $CF_3SO_3^-$ | |
| **8** | 16 | $CF_3SO_3^-$ | | **17** | 16 | $CF_3SO_3^-$ | |
| **9** | 18 | $CF_3SO_3^-$ | | **18** | 18 | $CF_3SO_3^-$ | |

intermolecular NH-bond interactions,[26] this result supporting our previous $^1$H NMR deductions.

The presence of the counteranion OTf in compounds **5–9** and **15–18**, and PTS in **1–4** and **10–14** is clearly confirmed by the two bands at 1250 cm$^{-1}$, $\nu_{as}(SO_3)$, and 1030 cm$^{-1}$, $\nu_s(SO_3)$, for the former, and at 1175 cm$^{-1}$, $\nu_{as}(SO_3)$, and 1015 cm$^{-1}$, $\nu_s(SO_3)$, for the latter.[25]

MALDI-TOF-MS spectra of complexes **1**, **7** and **11** show the peaks corresponding to the fragments $[Ag(Hpz^{2R(12)})]^+$, $[Ag(Hpz^{2R(14)})]^+$ and $[Ag(Hpz^{R(12)})]^+$, in agreement with a 1 : 1 metal/ligand stoichiometric ratio at $m/z$ 695.4, 751.4 and 435.2, respectively, as the most intense signal. A peak corresponding to the $[AgA + Na]^+$ fragment is also clearly distinguished. Unfortunately, the molecular ion peak $[M + A]^+$ (A = counteranion) could not be observed, thereby indicating that these fragments are not stable under MALDI conditions, in which the counteranion and one pyrazole ligand are lost under the applied laser irradiation. However, these facts suggest the high stability of the 1 : 1 species in all of the complexes studied.

### Crystal structures of complexes $[Ag(Hpz^{2R(1)})_2][OTf]$ (5) and $[Ag(Hpz^{R(1)})_2][PTS]$ (10)

All attempts to grow adequate crystals of the compounds with long-chained ligands for X-ray diffraction studies were unsuccessful. Therefore, we tried to obtain crystals of related compounds containing shorter chain ligands. In particular we were able to grow suitable crystals of $[Ag(Hpz^{2R(1)})_2][OTf]$ (**5**) and $[Ag(Hpz^{R(1)})_2][PTS]$ (**10**) by slow vapor diffusion of hexane into a dichloromethane solution and then solving their crystalline structures (Table 2).

The molecular structure of $[Ag(Hpz^{2R(1)})_2][OTf]$ (**5**) is depicted in Fig. 2, and Table S1† lists select bond distances and angles. The compound crystallises in the triclinic system, space group $P(-1)$. Because of minor disorder problems, the oxygen and fluorine atoms of the OTf counteranion were only refined isotropically (see Experimental section), this issue being previously observed in compounds containing this moiety.[27]

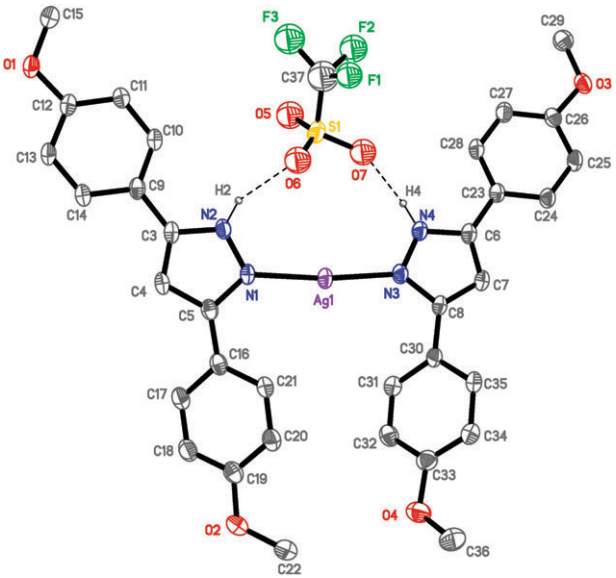


**Fig. 2** ORTEP plot of $[Ag(Hpz^{2R(1)})_2][CF_3SO_3]$ (**5**) with 35% probability. Hydrogen atoms, except for H2 and H4, have been omitted for clarity.

**Table 2** Crystal and refinement data for $[Ag(Hpz^{2R(1)})_2][OTf]$ (**5**) and $[Ag(Hpz^{R(1)})_2][PTS]$ (**10**)

| | **5** | **10** |
|---|---|---|
| Empirical formula | $[C_{34}H_{32}N_4O_4Ag][CF_3SO_3]$ | $[C_{20}H_{20}N_4O_2Ag][CH_3$-$p$-$C_6H_4SO_3]$ |
| Formula weight | 817.58 | 627.46 |
| Crystal system | Triclinic | Monoclinic |
| Space group | $P(-1)$ | $P2_1/c$ |
| Space group number | 2 | 14 |
| $a$/Å | 7.8645(4) | 10.223(1) |
| $b$/Å | 13.3014(7) | 21.903(1) |
| $c$/Å | 16.7157(9) | 12.946(1) |
| $\alpha$ (°) | 86.066(1) | — |
| $\beta$ (°) | 88.383(1) | 109.930(2) |
| $\gamma$ (°) | 87.054(1) | — |
| $V$/Å$^3$ | 1741.7(2) | 2725.1(3) |
| $Z$ | 2 | 4 |
| $T$/K | 296(2) | 296(2) |
| $F$(000) | 832 | 1280 |
| $\rho_c$/g cm$^{-3}$ | 1.559 | 1.529 |
| $\mu$/mm$^{-1}$ | 0.709 | 0.860 |
| Scan technique | ω and φ | ω and φ |
| Data collected | (−9, −15, −19) to (9, 15, 19) | (−12, −25, −15) to (11, 20, 15) |
| $\theta$ range (°) | 1.22 to 25.00 | 1.86 to 25.57 |
| Reflections collected | 17121 | 15883 |
| Independent reflections | 6106 ($R_{int}$ = 0.0248) | 4613 ($R_{int}$ = 0.0529) |
| Completeness to maximum $\theta$ (%) | 99.6 | 90.2 |
| Data/restraints/parameters | 6106/6/430 | 4613/0/349 |
| Observed reflections [$I > 2I\sigma(I)$] | 4633 | 2667 |
| $R^a$ | 0.0795 | 0.0448 |
| $R_{wF}{}^b$ | 0.2641 | 0.1499 |

$^a$ $\sum[|F_o| - |F_c|]/\sum|F_o|$. $^b$ $\{\sum[w(F_o{}^2 - F_c{}^2)^2]/\sum[w(F_o{}^2)^2]\}^{1/2}$.

 

The cationic unit shows a non-conventional "H" shape defined by two disubstituted pyrazole rings, bonded to the metal centre through the pyrazolic nitrogen. The coordination environment around the silver atom is almost linear with an N–Ag–N angle of 173.8(2)° and Ag–N1 and Ag–N3 distances of 2.127(5) Å and 2.117(5) Å, respectively, values similar to those observed in related compounds containing heterocyclic ligands.[28]

The phenyl rings from the two pyrazole substituents form dihedral angles of 29.6(2) and 0.9(2)°, and 4.6(2) and 37.5(2)° with their corresponding pyrazole planes, and are twisted 30.2(2) and 33.0(2)° between them. The complex exhibits a *cis*-orientation of the NH groups of both pyrazole ligands, as deduced by the torsion angle $\tau$ of 2.2(1)°, defined by the four nitrogen atoms (N1, N2, N3 and N4) of the two pyrazole ligands. The triflate counteranion is bonded through strong hydrogen bonds with the NH groups of both heterocycles, giving rise to an eight-membered metallocycle defined by the atoms O6–N2–N1–Ag–N3–N4–O7–S1 (Table S2†).

On a supramolecular level, the bispirazolyl-silver cationic units, bonded to their corresponding counteranion, are packed in parallel layers in the (1 1 1) direction. The cationic units adopt a face-to-face disposition, bonded through non-conventional hydrogen bonds of the type C–H···O of *ca.* 3.33 Å, so generating a 1D network along the *b* axis (Fig. 3a).

Besides, the 1D chains connect with neighbouring chains through new weak C–H···O interactions, producing double chains that are arranged through π···π interactions of *ca.* 3.64 Å between phenyl and pyrazole rings (Fig. 3b).

As the same time, the double chains are bonded through non-conventional C–H···O hydrogen bonds of 3.45 Å in a 2D network defined by layers which lie parallel to the (1 1 1) direction (Fig. 3c). Finally, new weak C–H···O interactions between layers can be considered as responsible for producing a 3D network (Table S2†).

The molecular structure of $[Ag(Hpz^{R(1)})_2][PTS]$ (**10**) is depicted in Fig. 4, and Table S3† lists selected bond distances and angles. The compound crystallises in the monoclinic system, space group $P2_1/c$. The asymmetric unit consists of two molecules orthogonally arranged (Fig. S1†), with two independent silver atoms, each lying on inversion centres.

The silver atom of each molecule is bonded to the two pyrazolic nitrogens in a linear coordination with Ag1–N1 and Ag2–N3 distances of 2.095(5) and 2.119(5) Å, respectively, and an N–Ag–N angle of 180°.

The cationic unit presents a high planarity, as deduced by the dihedral angles between the phenyl rings and its own pyrazole plane (dihedral angles 4.3(2) and 3.8(2)°). The alkyl chains are almost in the same plane as the pyrazole rings, with the two arms pointing out in opposite directions.

As a relevant difference to the structural features observed in **5**, it is noted that the two cationic entities exhibit a *trans*-NH group arrangement of the two pyrazole ligands, with a torsion angle, $\tau$, of 180°. They are bonded to their corresponding OTf counteranion through strong and bifurcated hydrogen bonds involving the N2 and N4 atoms of the NH pyrazolic rings, and the S1, O3 and S1A, O5A atoms of the two PTS counteranions (Table S4†), so generating a special "Z" molecular shape, also called a chair shape (Fig. 4).

On the other hand, the cationic entities $[Ag(Hpz^{R(1)})_2]^+$ are also H-bonded to their corresponding counteranion, giving

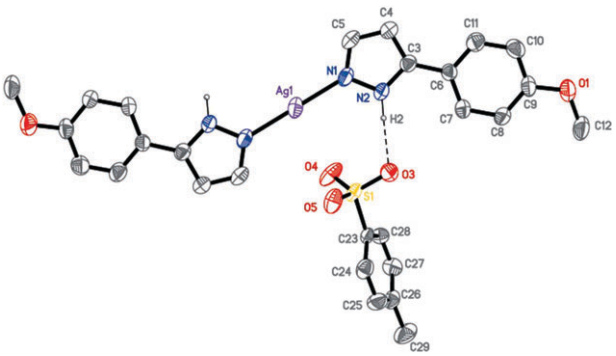


**Fig. 4** ORTEP plot of $[Ag(Hpz^{R(1)})_2][CH_3\text{-}p\text{-}C_6H_4SO_3]$ (**10**) with 30% probability. Hydrogen atoms, except for H2, and one entity of the asymmetric unit have been omitted for clarity (symmetry operations see Table S4†).

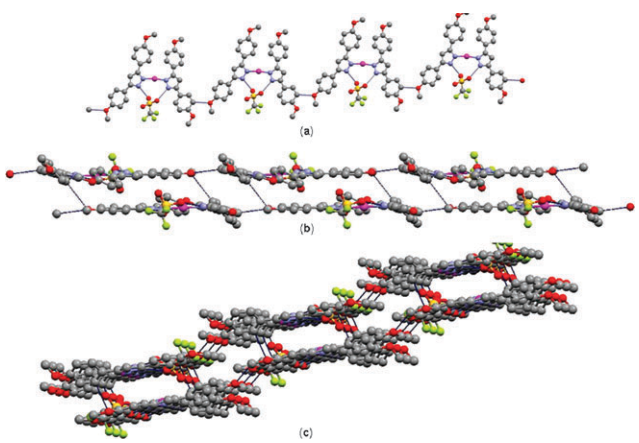


**Fig. 3** The crystal structure of **5**: (a) molecular chain along the *b* axis, (b) double chain and (c) layered 2D network parallel to the (1 1 1) direction.

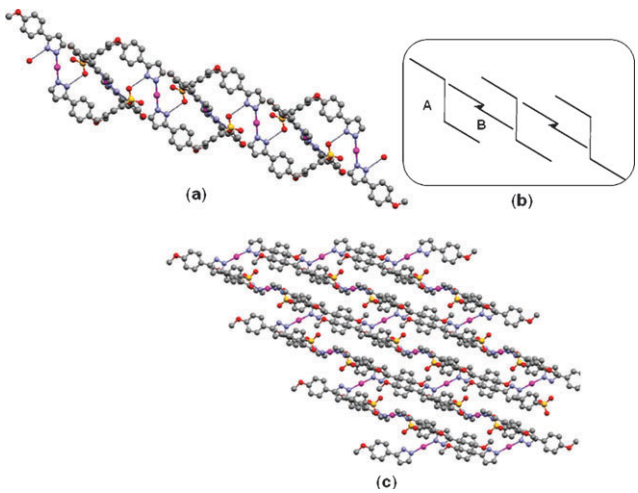


**Fig. 5** The crystal structure of **10**: (a) columns, (b) schematic representation of the A and B molecules in the asymmetric unit along (1 0 −1) direction, and (c) a corrugated layer.

rise to columns that exhibit Ag···Ag distances of 6.74 Å (Fig. 5a,b). Interactions of the type π···π between phenyl groups of neighbouring columns of 3.6–3.8 Å along the (1 0 −1) direction produce a corrugated layer (Fig. 5c). New C–H···O interactions between layers can also be considered to be responsible for a 3D network.

### Mesomorphic behaviour

The thermal behaviour of all the new complexes was determined using polarised light optical microscopy (POM) and differential scanning calorimetry (DSC) techniques. The nature of the mesophases was confirmed by using X-ray diffraction (XRD) at various temperatures. Table 3 summarises the thermal data.

The compounds of type **II** (**11–18**) were not mesomorphic, simply melting to the isotropic state.

By way of contrast, the complexes of type $\mathbf{I_{PTS}}$ (**1–4**) $[Ag(Hpz^{2R(n)})_2][PTS]$ displayed mesomorphic enantiotropic behaviour. On heating, SmA mesophases, characterised by their typical fan-shaped texture, were observed at *ca.* 100 °C (Fig. 6a). In addition to these mesophases, on cooling, SmC mesophases exhibiting sanded or broken-focal conic textures were also observed (Fig. 6b).

However the liquid crystal behaviour of the homologous counterparts containing OTf ($\mathbf{I_{OTf}}$) as the counteranion was restricted to those derivatives with $n$ = 12 (**6**) and $n$ = 14 (**7**), which again exhibited enantiotropic SmA mesophases (Fig. 6c).

The DSC thermograms of complexes **1–4** show on the first heating three endothermic peaks and on cooling three exothermic peaks assigned as follows.

For complexes **2** and **3**, with $n$ = 14 and $n$ = 16, respectively, the first two peaks from the solid–solid and solid–SmA mesophase transitions are followed by a third one with a lower enthalpy value, corresponding to the SmA–isotropic liquid transition. On cooling from the isotropic liquid, the first observed peak is due to the formation of an SmA mesophase and the second is related to a new mesophase identified as SmC. The last peak agrees with the crystallisation process. The calculated enthalpy values of all the processes are consistent with this assignment (Table 3).

**Fig. 6** Microphotographs of the textures on cooling observed by POM of (a) SmA phase for $[Ag(Hpz^{2R(18)})_2][CH_3\text{-}p\text{-}C_6H_4SO_3]$ (**4**) at 112 °C, (b) SmC phase for $[Ag(Hpz^{2R(18)})_2][CH_3\text{-}p\text{-}C_6H_4SO_3]$ (**4**) at 82 °C, and (c) SmA phase for $[Ag(Hpz^{2R(14)})_2][CF_3SO_3]$ (**7**) at 109 °C.

Complex **4** shows an analogous thermogram on heating; however, on cooling, the SmA–SmC transition observed by POM at *ca.* 85 °C was not detected. A related feature is observed for compound **1**, whose DSC thermogram on cooling shows only a peak corresponding to the formation of an SmA mesophase from the isotropic liquid, the transition from SmA to SmC mesophase being only detected by POM. In addition,

**Table 3** Phase behaviour of complexes **1–4**, **6** and **7** determined by POM and DSC

| | | | $T$/°C ($\Delta H$/kJ mol$^{-1}$) | | | | | | | | |
|---|---|---|---|---|---|---|---|---|---|---|---|
| $n$ | | Cycle | Cr | ⇄ | Cr′ | ⇄ | SmC | ⇄ | SmA | ⇄ | I |
| 12 | **1** | Heating | • | 61 (37.2) | • | | | 81 (11.1) | • | 140 (3.0) | • |
| | | Cooling | •[b] | 65[a] | | | • | 70[a] | • | 139 (−5.2) | • |
| 14 | **2** | Heating | • | 51 (25.8) | • | | | 88 (20.5) | • | 145 (6.6) | • |
| | | Cooling | • | 53 (−16.4) | | | • | 77 (−4.9) | • | 144 (−6.4) | • |
| 16 | **3** | Heating | • | 95 (26.2) | • | | | 105 (19.8) | • | 125 (6.0) | • |
| | | Cooling | • | 85 (−15.8) | | | • | 100 (−5.1) | • | 120 (−6.0) | • |
| 18 | **4** | Heating | • | 71 (95.5) | • | | | 104 (8.3) | • | 127 (3.3) | • |
| | | Cooling | • | 61 (−11.2) | | | • | 85[a] | • | 126 (−3.9) | • |
| 12 | **6** | Heating | • | | | | | 84 (30.8) | • | 155 (7.0) | • |
| | | Cooling | • | 55 (−15.0) | | | | | • | 153 (−7.3) | • |
| 14 | **7** | Heating | • | | | | | 97 (31.8) | • | 150 (7.6) | • |
| | | Cooling | • | 60 (−11.5) | | | | | • | 149 (−4.0) | • |

[a] Temperatures determined by POM. [b] crystal smectic glassy.

 

at 65 °C, the mobility of the SmC mesophase disappears, although the optical texture is maintained, this fact suggesting the formation of a crystal smectic glassy.

DSC thermograms for compounds **6** and **7** exhibit slight differences. On heating, they show two endothermic peaks, corresponding to the Cr–SmA and SmA–I transitions, and on cooling, two peaks related to the expected formation of the mesophase and crystallisation processes are observed.

The clear variations between the thermal behaviour of the $\mathbf{I_{PTS}}$ and $\mathbf{I_{OTf}}$ complexes evidence the influence of the counteranion on the mesomorphic properties, as already proposed in our previous work.[22] Therefore, at this point of the discussion, a further comparison of the thermal results of the complexes containing both the bulky (PTS, OTf) and small ($PF_6^-$, $NO_3^-$, $BF_4^-$) counteranions is considered interesting in order to shed light on the knowledge of the best structure–properties relationship (Scheme 2). In particular, the melting temperatures of the OTf derivatives are higher than those of their homologues with PTS, this fact suggesting stronger cation–anion interactions for the former. However, in the related compounds containing $PF_6^-$, $NO_3^-$ and $BF_4^-$, those with the bulkiest anion, $PF_6^-$, exhibit the higher melting temperatures, these results being associated to the most favourable packing produced by the spherical and bulky counteranion $PF_6^-$.[22]

On the other hand, within a given series of complexes, the melting point of the mesomorphic homologues increases with the chain length, *e.g.* between 81 and 105 °C for $\mathbf{I_{PTS}}$ and 84 and 97 °C for $\mathbf{I_{OTf}}$, the same way that it has also been found for $\mathbf{I_{BF_4}}$ between 64 and 70 °C, and $\mathbf{I_{NO_3}}$ between 40 and 68 °C.[22] By way of contrast for $\mathbf{I_{PF_6}}$ (whose melting point is, in general terms, higher than those of the homologues $\mathbf{I_{BF_4}}$ and $\mathbf{I_{NO_3}}$ due to the best intermolecular packing),[22] the increasing of the length chain causes a lowering of the melting point. Ignoring the behaviour of $\mathbf{I_{PF_6}}$, the increasing of this temperature with chain length could be explained by van der Waals interactions between chains, which should be more important than intermolecular core–core interactions.

The clearing point of the SmA phases decreases slightly in all cases with the chain length, independent of the counteranion, giving rise to a lower stability range of the SmA mesophase for the complexes with the longest chains.

All the above observations suggest that the melting transition may be well controlled by some of the intermolecular interactions and ionic forces discussed above, and that these can exert a greater effect than that of chain length alone.

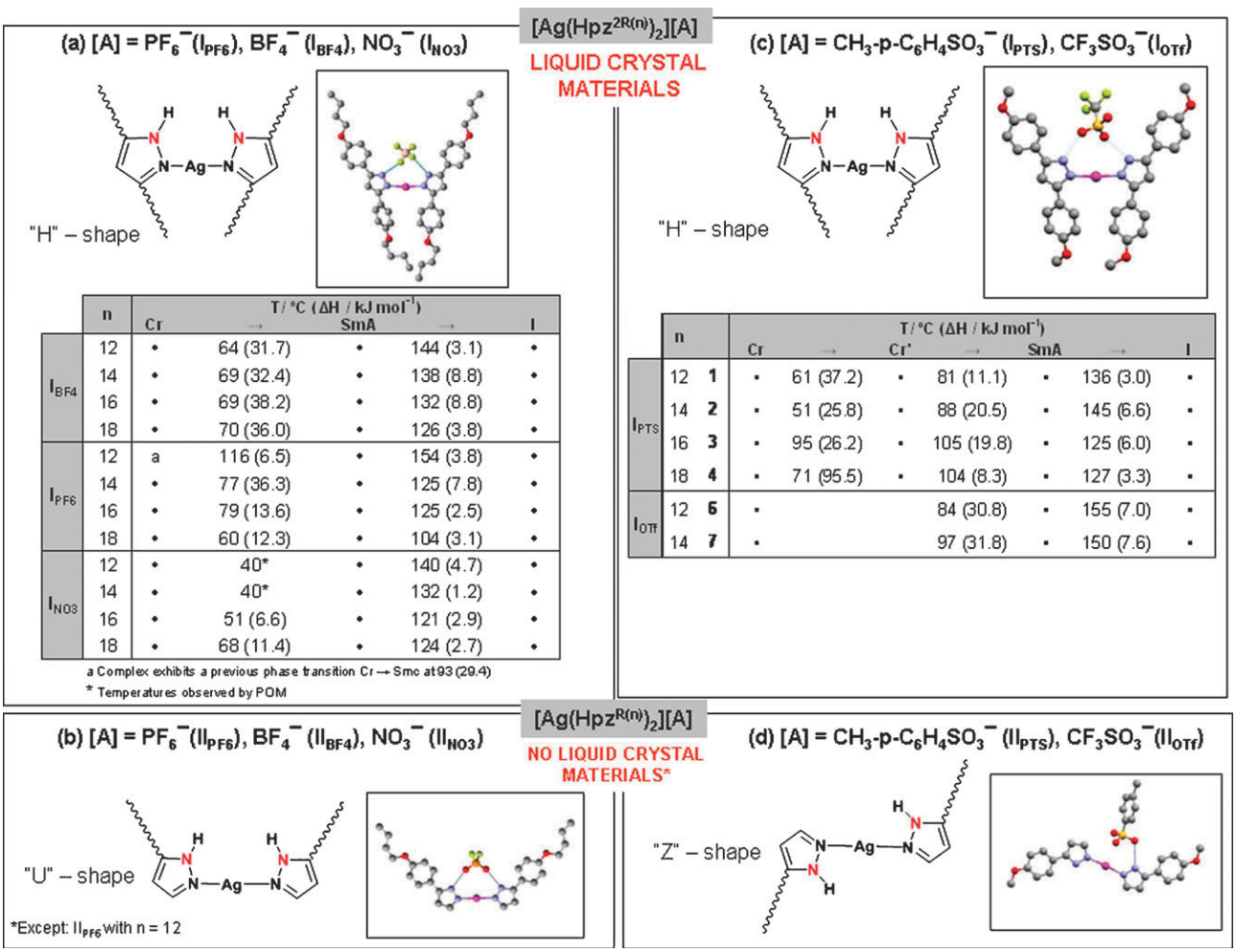


| | n | Cr | T / °C (ΔH / kJ mol⁻¹) | SmA | I |
|---|---|---|---|---|---|
| $I_{BF4}$ | 12 | • | 64 (31.7) | • 144 (3.1) | • |
| | 14 | • | 69 (32.4) | • 138 (8.8) | • |
| | 16 | • | 69 (38.2) | • 132 (8.8) | • |
| | 18 | • | 70 (36.0) | • 126 (3.8) | • |
| $I_{PF6}$ | 12 | a | 116 (6.5) | • 154 (3.8) | • |
| | 14 | • | 77 (36.3) | • 125 (7.8) | • |
| | 16 | • | 79 (13.6) | • 125 (2.5) | • |
| | 18 | • | 60 (12.3) | • 104 (3.1) | • |
| $I_{NO3}$ | 12 | • | 40* | • 140 (4.7) | • |
| | 14 | • | 40* | • 132 (1.2) | • |
| | 16 | • | 51 (6.6) | • 121 (2.9) | • |
| | 18 | • | 68 (11.4) | • 124 (2.7) | • |

a Complex exhibits a previous phase transition Cr → Smc at 93 (29.4)
* Temperatures observed by POM

| | n | | Cr | T / °C (ΔH / kJ mol⁻¹) | Cr' | SmA | I |
|---|---|---|---|---|---|---|---|
| $I_{PTS}$ | 12 | 1 | • | 61 (37.2) | • 81 (11.1) | • 136 (3.0) | • |
| | 14 | 2 | • | 51 (25.8) | • 88 (20.5) | • 145 (6.6) | • |
| | 16 | 3 | • | 95 (26.2) | • 105 (19.8) | • 125 (6.0) | • |
| | 18 | 4 | • | 71 (95.5) | • 104 (8.3) | • 127 (3.3) | • |
| $I_{OTf}$ | 12 | 6 | • | | 84 (30.8) | • 155 (7.0) | • |
| | 14 | 7 | • | | 97 (31.8) | • 150 (7.6) | • |

**Scheme 2** Molecular shapes and mesomorphic behaviour of complexes $[Ag(Hpz^{2R(n)})_2][A]$ (**I**) and $[Ag(Hpz^{R(n)})_2][A]$ (**II**): (a) and (b) ref. 22; (c) and (d) current work.

The compounds of type **II** with monosubstituted ligands (**11–18**) displayed non-mesomorphic behaviour analogous to that of the related compounds $\mathbf{II_{BF_4}}$, $\mathbf{II_{PF_6}}$ and $\mathbf{II_{NO_3}}$, with exception of the mesomorphism of $\mathbf{II_{PF_6}}$, bearing 12 carbon atoms on the alkyl chains (Scheme 2b,d).[22] These complexes exhibit bowl-shaped molecules, and the absence of liquid crystal properties is explained as a consequence of the decreasing interpenetration of the chains on the observed columnar arrangement followed by a decreasing anisotropy and therefore weaker core–core interactions.[22]

In the actual complexes $\mathbf{II_{PTS}}$ and $\mathbf{II_{OTf}}$, the "Z" molecular shape appears to be responsible for the absence of liquid crystalline properties. A similar behaviour was reported by Lee *et al.*[29] when considering the non-mesomorphic nature of cationic silver bis-benzimidazole complexes associated with their chair molecular shape. Selected complexes of the families $\mathbf{I_{PTS}}$ and $\mathbf{I_{OTf}}$ were subjected to temperature-dependent powder X-ray diffraction (XRD) measurements. The XRD patterns show in all cases two or three sharp peaks in the small angle region in a 1 : 1/2 : 1/3 ratio of the (0 0 1), (0 0 2) and (0 0 3) reflections, corresponding to a lamellar structure, and a broad halo at *ca.* 4.5 Å owing to the liquid-like order of the molten alkyl chains. This diffraction pattern is in agreement with the lamellar structure of the SmA mesophase assigned by POM. Table 4 summarises the results of the X-ray diffraction patterns of **2**, **4** and **7**, selected as representative examples.

On cooling, the XRD diffractograms of compounds of type $\mathbf{I_{PTS}}$ confirmed the presence of two mesophases. So, for example, for complex **2** at 120 °C, the small angle peaks at 2.5 and 4.8°, and the two new ones at 2.4 and 4.6° at 70 °C with a reciprocal space ratio of 1 : 2, indexed to the (0 0 1) and (0 0 2) reflections, are typical of a layered arrangement. The variation of the lamellar periodicity *d* at 70 °C with respect to that of the corresponding diffractogram at 120 °C (Table 4) evidences a SmA–SmC transition, which had also been registered by DSC and observed by POM. It is important to note that the layer spacing of the SmA mesophase is smaller than that of the SmC phase, this feature being attributed to the loss of conformational freedom at low temperature, which causes the more extended chains to overcome the effect of tilting.[18,22,30]

## Photophysical studies

Photoluminescence studies of selected complexes of type **I** (**1**, **7**) and type **II** (**11**, **15**) were carried out. All selected compounds, **1**, **7**, **11** and **15**, are luminescent at room temperature, both in the solid state and in solution. Mesomorphic complexes **1** and **7** were also luminescent in the liquid crystal

**Table 4** X-Ray diffraction data of mesomorphic complexes

| *n* | Complex | *T*/°C | Mesophase | Position (°)/2$\theta$ | *d*-spacing/Å | Miller indices (*hkl*) |
|---|---|---|---|---|---|---|
| 14 | **2** | 135 | SmA | 2.4 | 36.2 | (001) |
| | | | | 4.8 | 18.5 | (002) |
| | | | | 7.0 | 12.0 | (003) |
| | | | | 19.3 | 4.6 | [a] |
| | | 120[b] | SmA | 2.5 | 36.3 | (001) |
| | | | | 4.8 | 18.5 | (002) |
| | | | | 19.8 | 4.5 | [a] |
| | | 70[b] | SmC | 2.4 | 37.0 | (001) |
| | | | | 4.6 | 19.0 | (002) |
| | | | | 19.2 | 4.6 | [a] |
| 18 | **4** | 125 | SmA | 2.3 | 38.2 | (001) |
| | | | | 4.6 | 19.3 | (002) |
| | | | | 18.9 | 4.7 | [a] |
| | | 120[b] | SmA | 2.3 | 39.1 | (001) |
| | | | | 18.7 | 4.7 | [a] |
| | | 80[b] | SmC | 2.1 | 42.7 | (001) |
| | | | | 19.4 | 4.6 | [a] |
| 14 | **7** | 100 | SmA | 2.4 | 36.5 | (001) |
| | | | | 4.8 | 18.3 | (002) |
| | | | | 7.1 | 12.3 | (003) |
| | | | | 20.1 | 4.3 | [a] |

[a] Halo of the molten alkoxy chains. [b] On cooling.

**Table 5** Optical data for compounds **1**, **7**, **11** and **15** in chloroform solution at room temperature

| Compound | $\lambda_{max}$ abs./nm | $\varepsilon$/L mol$^{-1}$cm$^{-1}$ | [Conc.]/10$^{-6}$ M | $\lambda_{emis}$/nm ($\lambda_{exc}$ = 274 nm) | $\Delta\lambda$/nm[a] |
|---|---|---|---|---|---|
| $Hpz^{2R(12)}$ | 267 | 55 063 | 3.24 | 362[b] | 95 |
| **1** | 270 | 57 500 | 1.00 | 380 | 110 |
| **7** | 270 | 38 900 | 1.00 | 393 | 123 |
| $Hpz^{R(12)}$ | 260 | 62 231 | 2.25 | 362[b] | 101 |
| **11** | 260 | 97 960 | 1.00 | 320 | 60 |
| **15** | 265 | 66 300 | 1.00 | 327 | 62 |

[a] Stokes shift in chloroform. [b] $\lambda_{exc}$ = 261 nm.

 

**Table 6** Optical data for compounds **1**, **7**, **11** and **15** as solid samples at room temperature

| Compound | $\lambda_{max}$ exc./nm | $\lambda_{emis}$/nm | $\lambda_{emis}$/nm ($\lambda_{exc}$ = 360 nm) | Color[a] | Color ($\lambda_{exc}$ = 366 nm) UV lamp |
|---|---|---|---|---|---|
| **1** | 265 | 352 | 372 | White | Orange |
| **7** | 265 | 386 | 398 | White | Orange |
| **11** | 265 | 394 | 455 | White | Orange |
| **15** | 265 | 328 | 450 | White | Pale orange |

[a] Solid powder samples.



state, which has been proved by variable-temperature luminescence studies.

**Solution studies.** Absorption UV-vis spectra were measured in $CHCl_3$ solutions (*ca.* $10^{-6}$ M). In all cases, a broad absorption band in the region of 240–320 nm was observed, with the maximum centered at *ca.* 270 nm for compounds **1** and **7**, and at *ca.* 265 nm for **11** and **15**. This band, associated with a $\pi$–$\pi^*$ electronic transition of the pyrazole group,[6] is slightly bathochromically-shifted with respect to the free ligand but it is not modified by the different counteranions (Table 5).

Compounds **I** exhibit a broad fluorescence band in the near-UV blue region. The band, attributed to a ligand-centered transition (LCT), was red shifted to respect to that of the free ligand ($\lambda_{emis}$ = 362 nm), this shift depending on the counteranion nature (Table 5). So, for complexes **1** with PTS and **7** with OTf, it was observed at 380 nm (Stokes shift 110 nm) and 393 nm (Stokes shift 123 nm). By way of contrast, the emission band of complexes **11** and **15** was blue-shifted, decreasing the Stokes shift *ca.* 40 nm with respect to the free ligand (Table 5).

**Solid studies.** The emission spectra of complexes **1** and **7** exhibit a broad band from 300 to 500 nm ($\lambda_{exc}$ = 265 nm), attributed to a ligand-centered transition (Table 6). When an excitation of 360 nm was used, a second lower intensity emission band, corresponding to a metal-centered charge transfer (MLCT), was registered.[22] Analogous results were obtained for complexes of type **II** (**11** and **15**).

The fluorescence emission of compounds in the solid state corresponding to an LCT transition is blue-shifted with respect to that observed in solution, the same way previously observed for complexes $\mathbf{I_{BF_4}}$, $\mathbf{I_{PF_6}}$ and $\mathbf{I_{NO_3}}$.[22] In contrast, for complexes $\mathbf{II_{PTS}}$ and $\mathbf{II_{OTf}}$ (**11** and **15**), this band is red-shifted, the emission value being dependent on the counteranion nature.

The differences in the luminescence behaviour of complexes of type **I** and **II** in the solid state can be related to their different molecular and structural features. Therefore, it is suggested that the luminescent properties of complexes can be modulated by modifying either the nature of the counteranion or the substitution on the pyrazole ligand, which is in fact responsible for the "H" (type **I**) or "Z" (type **II**) molecular shapes found for these complexes.

**Variable temperature studies.** In order to prove the luminescent behaviour of the compounds in the liquid crystal state, the emission spectra of **1** and **7** were studied at different temperatures from the solid state to the isotropic liquid. In both cases, the fluorescence spectra were also registered on cooling from the isotropic liquid until the solidification temperature (Fig. 7). In this way, we could observe the fluorescence emission as a function of temperature, as well as the aggregation state of the compounds.

On heating, the behaviour of the emission band is similar for both compounds, showing that the intensity of the fluorescence decreases upon the temperature increasing, and it almost disappears at the clearing temperature. The pattern of the band is maintained across the temperature range used on heating and on cooling (Fig. 7). The emission maximum is maintained in both the solid state and the liquid crystal state, which is indicative that neither the structural changes nor the mesophase viscosity affect the excited state.

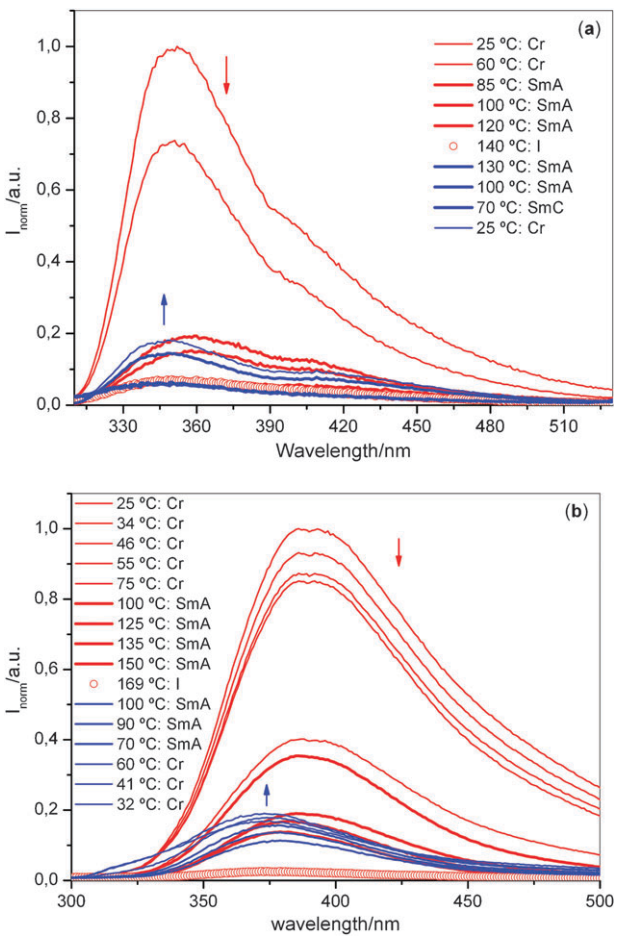


**Fig. 7** Fluorescence spectra of compounds (a) **1** and (b) **7** in the solid state as a function of temperature ($\lambda_{exc}$ = 274 nm). The spectra and the temperature list follow the same top-to-bottom order (on cooling) and bottom-to-top order on heating.

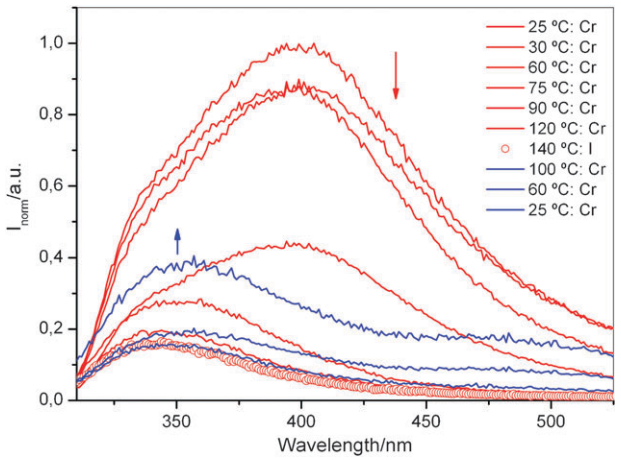


**Fig. 8** Fluorescence spectra of compound **11** in the solid state as a function of temperature ($\lambda_{exc}$ = 274 nm). The spectra and the temperature list follow the same top-to-bottom order (on cooling) and bottom-to-top order on heating.

The above results allow us to establish that the liquid crystal state does not quench the emission.

On cooling, the emission tends to be recovered and increases in intensity, although the total fluorescence emission is not rescued. As an explanation of this result, it is possible to suggest that the crystalline solid obtained after the crystallisation process from the mesophase is different to that of the initial solid before the first heating, which is in agreement with the slight shift of the emission maximum from the starting to final solid that is clearly observed in complex $[Ag(Hpz^{2R(14)})_2][OTf]$ (**7**) (Fig. 7b).

For comparative purposes, the variable temperature studies of non-mesomorphic compound $[Ag(Hpz^{R(12)})_2][PTS]$ (**11**) were also performed (Fig. 8). The most appreciable difference with respect to the results obtained from the above-mentioned mesomorphic complexes **1** and **7** (Fig. 7) is related to the shift of the emission maximum to a lower wavelength when the temperature is increased, indicating that the excited state is slightly modified.

## Experimental

### Materials and physical measurements

All commercial reagents were used as supplied. The 3-(4-alkyloxyphenyl)-1*H*-pyrazoles ($Hpz^{R(n)}$) and 3,5-bis(4-alkyloxyphenyl)-1*H*-pyrazoles ($Hpz^{2R(n)}$) (R = $C_6H_4OC_nH_{2n+1}$; $n$ = 1, 12, 14, 16, 18) were prepared by procedures described in previous work.[31,32] Commercial solvents were dried prior to use.

Elemental analyses for carbon, hydrogen and nitrogen were carried out by the Microanalytical Service of Complutense University. IR spectra were recorded on a FTIR Thermo Nicolet 200 spectrophotometer with samples as KBr pellets in the 4000–400 $cm^{-1}$ region: vs (very strong), s (strong), m (medium), w (weak).

$^1H$ NMR spectra were performed at room temperature on a Bruker DPX-300 spectrophotometer (NMR Service of Complutense University) from solutions in $CDCl_3$. Chemical shifts $\delta$ are listed relative to $Me_4Si$ using the signal of the deuterated solvent as reference (7.26 ppm), and coupling constants $J$ are in Hertz. Multiplicities are indicated as s (singlet), d (doublet), t (triplet), m (multiplet), br s (broad signal). The $^1H$ chemical shifts and coupling constants are accurate to ±0.01 ppm and ±0.3 Hz, respectively.

Phase studies were carried out by optical microscopy using an Olympus BX50 microscope equipped with a Linkam THMS 600 heating stage. The temperatures were assigned on the basis of optic observations with polarised light.

Measurements of the transition temperatures were made using a Perkin-Elmer Pyris 1 differential scanning calorimeter with the sample (1–4 mg) sealed hermetically in aluminium pans and with a heating or cooling rate of 5–10 K $min^{-1}$.

The X-ray diffractograms at variable temperature were recorded on a Panalytical X'Pert PRO MPD diffractometer in a θ-θ configuration equipped with a Anton Paar HTK1200 heating stage (X-Ray Diffraction Service of Complutense University).

Absorption spectra were recorded on a Shimadzu UV-2501PC spectrophotometer and fluorescence emissions were measured on a Horiba-Jobin-Yvon SPEX Fluorolog 3.22 spectrofluorimeter equipped with a ThermoNeslab RTE7 bath. The linearity of the fluorescence emission *vs.* concentration was checked in the concentration range used ($10^{-4}$–$10^{-6}$ M). A correction for absorbed light was performed when necessary. All spectrofluorimetric studies were performed as follows: stock solutions of the ligands (*ca.* $10^{-3}$ M) were prepared by dissolving an appropriate amount of the ligand in a 50 mL volumetric flask and diluting to the mark with chloroform HPLC or UVA-sol grades. Fluorescence spectra of solid samples were recorded on the spectrofluorimeter exciting the solid compounds at appropriated $\lambda$ (nm) using a fiber-optics devices connected to the spectrofluorimeter. The emission spectra as a function of the temperature were recorded in the 300–800 nm range using a fiber optic system connected to the spectrofluorimeter, and the solid samples were heated over a hot plate with an external temperature control provided by a digital thermo par.

The MALDI-TOF-TOF-MS spectra of complexes **1**, **7** and **11** were acquired on an Applied Biosystems 4700 proteomics analyser using an $N_2$ laser at 337 nm in the University of Vigo, BIOSCOPE Group (Applied Biosystems, Foster City, CA, USA). MALDI mass spectra were acquired in positive ion reflectron mode, with an accelerating voltage of 20 kV, an ion extraction delay of 80 ns, a grid voltage of 15 kV, and a guide wire voltage of 40 V. The MALDI mass spectrum for each sample was based on an average of 600 laser shots. All the data were processed using the Data Explorer software package (Applied Biosystems). All compounds were spotted on the MALDI target plate (2 μg $\mu L^{-1}$) without any MALDI-matrix, dissolving the compounds in acetonitrile or chloroform.

### Crystallographic structure determination

Data collection for both compounds **5** and **10** was carried out at room temperature on a Bruker Smart CCD diffractometer using graphite-monochromated Mo-$K_\alpha$ radiation ($\lambda$ = 0.71073 Å), operating at 50 kV and 25 mA. Data were

 

collected over a hemisphere of the reciprocal space by combination of three exposure sets. Each exposure of 20 s covered 0.3° in $\omega$.

The cell parameters were determined and refined by a least-squares fit of all reflections.

The first 50 frames were recollected at the end of the data collection to monitor crystal decay, and no appreciable decay was observed.

A summary of the fundamental crystal and refinement data is given in Table 2. For **5**, a semi-empirical absorption correction was applied.

The structures were solved by direct methods and conventional Fourier techniques and refined by applying full-matrix least-squares on $F^2$,[33] with anisotropic thermal parameters for the non-hydrogen atoms, with some exceptions. For **5**, due to a non-resolvable positional disorder found in the OTf group, the O and F atoms were refined isotropically with restrained S–O and C–F distances.

The hydrogen atoms were included at their calculated positions determined by molecular geometry and refined riding on the corresponding carbon atoms, except for the H2 and H4 bonded to N2 and N4 atoms, which were located from the Fourier map included and were refined riding on the corresponding nitrogen atoms for **5** and not refined for **10**.

### Preparation of the complexes of the types I and II

To a solution of the corresponding 3,5-bis(4-alkyloxyphenyl)-1*H*-pyrazole ($Hpz^{2R(n)}$) or 3-(4-alkyloxyphenyl)-1*H*-pyrazole ($Hpz^{R(n)}$) in dry tetrahydrofuran was added AgA in a 2:1 molecular ratio under a dinitrogen atmosphere (Scheme 1). The mixture was stirred for 24 h in the absence of light, and then filtered through Celite®. The clear filtrate was removed *in vacuo* and the residue was dissolved in dichloromethane. The addition of hexane gave rise to a colorless solid, which was filtered off, washed with hexane and dried *in vacuo*.

Spectroscopic IR and $^1$H NMR data are given for **1**, **6** (type **I**) and **11**, **15** (type **II**) as selected representative examples of each type of compound. Data for the other homologues are essentially identical. Yields and analytical data are collected in Table S5 as ESI.†

$[Ag(Hpz^{2R(12)})_2][PTS]$ (**1**). $\nu_{max}$(KBr)/cm$^{-1}$ 3230m (NH), 1615s (C=N) + (C=C), 1175vs and 1035s ($SO_3$). $\delta_H$ (300 MHz; $CDCl_3$; $Me_4Si$) 0.88 (12 H, t, $^3J_{H,H}$ 6.3, $CH_3$), 1.27 (72 H, m, $CH_2$), 1.78 (8 H, m, $CH_2$), 2.39 (3 H, s, $CH_3$ PTS), 3.91 (8 H, t, $^3J_{H,H}$ 6.3, $OCH_2$), 6.67 (2 H, s, C(4)H), 6.76 (8 H, d, $^3J_{H,H}$ 8.3, $H_m$), 7.24 (2 H, d, $^3J_{H,H}$ 8.0, $H_m$ PTS), 7.64 (8 H, d, $^3J_{H,H}$ 8.3, $H_o$), 7.96 (2 H, d, $^3J_{H,H}$ 8.0, $H_o$ PTS).

$[Ag(Hpz^{2R(12)})_2][OTf]$ (**6**). $\nu_{max}$(KBr)/cm$^{-1}$ 3231m (NH), 1616m (C=N) + (C=C), 1254vs and 1030s ($SO_3$). $\delta_H$ (300 MHz; $CDCl_3$; $Me_4Si$) 0.88 (12 H, t, $^3J_{H,H}$ 6.4, $CH_3$), 1.27 (72 H, m, $CH_2$), 1.81 (8 H, m, $CH_2$), 3.97 (8 H, t, $^3J_{H,H}$ 6.5, $OCH_2$), 6.75 (2 H, s, C(4)H), 7.00 (8 H, d, $^3J_{H,H}$ 8.7, $H_m$), 7.71 (8 H, d, $^3J_{H,H}$ 8.7, $H_o$).

$[Ag(Hpz^{R(12)})_2][PTS]$ (**11**). $\nu_{max}$(KBr)/cm$^{-1}$ 3150w (NH), 1613m (C=N) + (C=C), 1178vs and 1037s ($SO_3$). $\delta_H$ (300 MHz; $CDCl_3$; $Me_4Si$) 0.88 (6 H, t, $^3J_{H,H}$ 6.7, $CH_3$), 1.27 (36 H, m, $CH_2$), 1.80 (4 H, m, $CH_2$), 2.51 (3 H, s, $CH_3$ PTS), 3.96 (4 H, t, $^3J_{H,H}$ 6.6, $OCH_2$), 6.54 (2 H, d, $^3J_{H,H}$ 2.3, C(4)H), 6.88 (4 H, d, $^3J_{H,H}$ 8.8, $H_m$), 7.21 (2 H, d, $^3J_{H,H}$ 8.0, $H_m$ PTS), 7.63 (2 H, d, $^3J_{H,H}$ 2.3, C(5)H), 7.63 (4 H, d, $^3J_{H,H}$ 8.8, $H_o$), 7.89 (2 H, d, $^3J_{H,H}$ 8.0, $H_o$ PTS)

$[Ag(Hpz^{R(12)})_2][OTf]$ (**15**). $\nu_{max}$(KBr)/cm$^{-1}$ 3125w (NH), 1613m (C=N) + (C=C), 1250vs and 1028s ($SO_3$). $\delta_H$ (300 MHz; $CDCl_3$; $Me_4Si$) 0.88 (6 H, t, $^3J_{H,H}$ 6.5, $CH_3$), 1.27 (36 H, m, $CH_2$), 1.80 (4 H, m, $CH_2$), 3.97 (4 H, t, $^3J_{H,H}$ 6.3, $OCH_2$), 6.59 (2 H, br s, C(4)H), 6.93 (4 H, d, $^3J_{H,H}$ 8.0, $H_m$), 7.58 (4 H, d, $^3J_{H,H}$ 8.0, $H_o$), 7.68 (2 H, br s, C(5)H).

## Conclusions

Mesomorphism of ionic silver complexes of type **I** $[Ag(Hpz^{2R(n)})_2][A]$, containing disubstituted pyrazole ligands, has been established on the basis of the adequation of the "H" molecular shape of their cationic entities to achieve the supramolecular ordering in the liquid crystal state. The mesophases are controlled by inter-chain interactions over the core–core interactions, their stability being favoured by the presence of bulky and coordinating counteranions like PTS and OTf.

The absence of mesomorphic properties of the related monosubstituted pyrazole compounds (type **II**) was also rationalized in terms of the unfavourable "Z" or "U" molecular shape of their cationic unities to achieve the ordering of mesophases.

All complexes of types **I** and **II** exhibit luminescence in the solid state and in solution at room temperature, this behaviour being independent of substitution in the pyrazole ring. By way of contrast, the presence of di- or monosubstituted pyrazole ligands was reflected both in red or blue fluorescence shifts with respect to that of their corresponding free ligand in the order OTf > PTS, and in the fluorescence range (370–393 and 320–364 nm) for **I** and **II**, respectively.

Fluorescence was also maintained in the liquid crystalline state for complexes **I**.

In summary, we have established that the luminescent and liquid crystalline properties of $[Ag(L)_2][A]$ ($L$ = $Hpz^{2R(n)}$ or $Hpz^{R(n)}$) can be modulated by controlling both the counter-anion nature and substitution on the pyrazole ligand.

## Acknowledgements

We thank the Secretaría de Estado de Investigación (Dirección General de Investigación) del Ministerio de Ciencia e Innovación of Spain, project CTQ2006-13344/BQU, and Universidad Complutense de Madrid (Spain), project UCM2008-910300, for financial support.

C. L. is grateful to InOu-Universidade de Vigo at Ourense Campus, Galicia (Spain) for financial support through project 2009K914122P64702 and thanks INCITE, Xunta de Galicia (Spain) for the Isidro Parga Pondal Research program. Masters student Sabina Rodriguez and Dr Laura Rodriguez are kindly acknowledged for helping with some initial fluorescence measurements.

## References

1 A. S. Matharu, S. Jeeva and P. S. Ramanujam, *Chem. Soc. Rev.*, 2007, **36**, 1868–1880; S. Laschat, A. Baro, N. Steinke, F. Giesselmann, C. Hägele, G. Scalia, R. Judele, E. Kapatsina,

S. Sauer, A. Schreivogel and M. Tosoni, *Angew. Chem., Int. Ed.*, 2007, **46**, 4832–4887; M. O'Neill and S. M. Kelly, *Adv. Mater.*, 2003, **15**, 1131–1146; J. Hanna, *Opto-Electron. Rev.*, 2005, **13**, 259–267.
2 F. Camerel, J. Barberá, J. Otsuki, T. Tokimoto, Y. Shimazaki, L.-Y. Chen, S.-H. Liu, M.-S. Lin and C.-C. Wu. R. Ziezzel, *Adv. Mater.*, 2008, **20**, 3462–3467.
3 T. Yasuda, H. Ooi, J. Morita, Y. Akama, K. Minoura, M. Funashashi, T. Shimomura and T. Kato, *Adv. Funct. Mater.*, 2009, **19**, 411–419.
4 S. Suárez, O. Mamula, D. Imbert, C. Piguet and J.-C. G. Bünzli, *Chem. Commun.*, 2003, 1226–1227.
5 K. Binnemans, *J. Mater. Chem.*, 2009, **19**, 448–453; K. Binnemans, *Chem. Rev.*, 2005, **105**, 4148–4204.
6 P. Ovejero, M. J. Mayoral, M. Cano and M. C. Lagunas, *J. Organomet. Chem.*, 2007, **692**, 1690–1697.
7 R. Bayón, S. Coco and P. Espinet, *Chem.–Eur. J.*, 2005, **11**, 1079–1085.
8 C. Piguet, J.-C. G. Bünzli, B. Donnio and D. Guillon, *Chem. Commun.*, 2006, 3755–3768.
9 E. Terazzi, S. Suarez, S. Torelli, H. Nozary, D. Imbert, O. Mamula, J. P. Rivera, E. Guillet, J. M. Benech, G. Bernardinelli, R. Scopelliti, B. Donnio, D. Guillon, J.-C. G. Bünzli and C. Piguet, *Adv. Funct. Mater.*, 2006, **16**, 157–168.
10 A. Escande, L. Guénée, H. Nozary, G. Bernardinelli, F. Gumy, A. Aebischer, J.-C. G. Bünzli, B. Donnio, D. Guillon and C. Piguet, *Chem.–Eur. J.*, 2007, **13**, 8696–8713.
11 Y. T. Yang, K. Driesen, P. Nockemann, K. Van Hecke, L. Van Meervelt and K. Binnemans, *Chem. Mater.*, 2006, **18**, 3698–3704.
12 Y. Galyametdinov, A. A. Knyazev, V. I. Dzhabarov, T. Cardinaels, K. Driesen, C. Görller-Walrand and K. Binnemans, *Adv. Mater.*, 2008, **20**, 252–257.
13 M. Ghedini, D. Pucci, A. Crispini, A. Bellusci, M. La Deda, I. Aiello and T. Pugliese, *Inorg. Chem. Commun.*, 2007, **10**, 243–246.
14 M.-H. Qi and G.-F. Liu, *J. Mater. Chem.*, 2003, **13**, 2479–2484.
15 A. Santoro, A. C. Whitwood, J. A. Gareth Williams, V. N. Kozhevnikov and D. W. Bruce, *Chem. Mater.*, 2009, **21**, 3871–3882; V. M. Kozhevnikov, B. Donnio and D. W. Bruce, Angew. Chem., *Angew. Chem., Int. Ed.*, 2008, **47**, 6286–6289.
16 K. Venkatesan, P. H. J. Kouwer, S. Yagi, P. Müller and T. M. Swager, *J. Mater. Chem.*, 2008, **18**, 400–407.
17 D. Pucci, I. Aiello, A. Bellusci, A. Crispini, M. Ghedini and M. La Deda, *Eur. J. Inorg. Chem.*, 2009, 4274–4281.
18 E. Cavero, S. Uriel, P. Romero, J. L. Serrano and R. Giménez, *J. Am. Chem. Soc.*, 2007, **129**, 11608–11618.
19 A. Kishimura, T. Yamashita, K. Yamaguchi and T. Aida, *Nat. Mater.*, 2005, **4**, 546–549.
20 D. Pucci, G. Barberio, A. Bellusci, A. Crispini, B. Donnio, L. Giorgini, M. Ghedini, M. La Deda and E. Ildyko Szerb, *Chem.–Eur. J.*, 2006, **12**, 6738–6747.
21 S. Coco, C. Cordovilla, C. Domínguez and P. Espinet, *Dalton Trans.*, 2008, 6894–6900; J. Arias, M. Bardají and P. Espinet, *Inorg. Chem.*, 2008, **47**, 3559–3567.
22 M. J. Mayoral, P. Ovejero, J. A. Campo, J. V. Heras, E. Pinilla, M. R. Torres, C. Lodeiro and M. Cano, *Dalton Trans.*, 2008, 6912–6924.
23 M. L. Gallego, P. Ovejero, M. Cano, J. V. Heras, J. A. Campo, E. Pinilla and M. R. Torres, *Eur. J. Inorg. Chem.*, 2004, 3089–3098.
24 M. Cano, J. V. Heras, M. Maeso, M. Alvaro, R. Fernández, E. Pinilla, J. A. Campo and A. Monge, *J. Organomet. Chem.*, 1997, **534**, 159–172; M. Cano, J. A. Campo, J. V. Heras, J. Lafuente, C. Rivas and E. Pinilla, *Polyhedron*, 1995, **14**, 1139–1147.
25 K. Nakamoto, *Infrared and Raman Spectra of Inorganic and Coordination Compounds*, John Wiley & Sons, New York, 5th edn, 1997.
26 J. Barberá, C. Cativiela, J. L. Serrano and M. M. Zurbano, *Liq. Cryst.*, 1992, **11**, 887–897.
27 M. C. Torralba, M. Cano, J. A. Campo, J. V. Heras, E. Pinilla, M. R. Torres, J. Perles and C. Ruiz-Valero, *J. Organomet. Chem.*, 2006, **691**, 2614–2622; M. L. Gallego, M. Cano, J. A. Campo, J. V. Heras, E. Pinilla, M. R. Torres, P. Cornago and R. M. Claramunt, *Eur. J. Inorg. Chem.*, 2005, 4370–4381.
28 P. Ovejero, M. J. Mayoral, M. Cano, J. A. Campo, J. V. Heras, E. Pinilla and M. R. Torres, *J. Organomet. Chem.*, 2007, **692**, 4093–4105.
29 C. K. Lee, K.-M. Hsu, C.-H. Tsai, C. K. Lai and I. J. B. Lin, *Dalton Trans.*, 2004, 1120–1126.
30 M. J. Baena, J. Barberá, P. Espinet, A. Ezcurra, M. B. Ros and J. L. Serrano, *J. Am. Chem. Soc.*, 1994, **116**, 1899–1906.
31 M. C. Torralba, M. Cano, J. A. Campo, J. V. Heras, E. Pinilla and M. R. Torres, *Inorg. Chem. Commun.*, 2006, **9**, 1271–1275; M. C. Torralba, M. Cano, J. A. Campo, J. V. Heras, E. Pinilla and M. R. Torres, *Inorg. Chem. Commun.*, 2002, **5**, 887–890.
32 M. C. Torralba, M. Cano, S. Gomez, J. A. Campo, J. V. Heras, J. Perles and C. Ruiz-Valero, *J. Organomet. Chem.*, 2003, **682**, 26–34; M. C. Torralba, M. Cano, J. A. Campo, J. V. Heras, E. Pinilla and M. R. Torres, *J. Organomet. Chem.*, 2002, **654**, 150–161.
33 G. M. Sheldrick, *SHELXL-97, Program for refinement of crystal structures*, University of Göttingen, Germany, 1997.



 